A Novel Permanent Magnet Motor with Doubly Salient Structure

Yuefeng Liao, *Member, IEEE*, Feng Liang, *Member, IEEE*, and Thomas A. Lipo, *Fellow, IEEE*

***Abstract*—A new type of doubly salient machine is presented in which the field excitation is provided by nonrotating Permanent Magnets. This doubly salient permanent magnet (DSPM) motor is shown to be kindred to square waveform permanent magnet brushless dc motors. Linear and nonlinear analyses are made to investigate the characteristics of this new type of PM motor. A prototype DSPM motor is designed and comparisons made between this new type of motor and the induction motor. It is shown that by fully exploiting modern high energy PM material and the doubly salient structure, the DSPM motor can offer superior performance over existing motors in terms of efficiency, torque density, torque-to-current ratio, torque-to-inertia ratio etc., while retaining a simple structure amenable to automated manufacture.**

I. Introduction

THE Variable Reluctance Motor (VRM) employing a doubly salient structure has been the focus of intensive research efforts during the past decade. Their torque production, design features, and control characteristics have been well explored [1]–[4]. In particular, the inherent fault-tolerant feature of this machine, among other merits claimed by its proponents, has been well demonstrated, and the variable reluctance motor is becoming a prime candidate for reliability-premium applications [5].

The VRM is, fundamentally, only one of a class of singly excited electromechanical energy conversion devices. Unlike doubly excited electrical machines, the lack of a separate field excitation winding in the VRM contributes to the structural simplicity and the inherent high reliability of the VRM drive. However, this feature also gives rise to a number of problems as viewed from the point of view of energy conversion. First, the variable reluctance action necessitates the use of only one of two possible torque producing zones. That is, motoring torque can be produced only when a rotor pole is entering the region occupied by a given phase, i.e., when the inductance is increasing. Only braking torque can be produced if the phase is energized while the pole is leaving the aligned, maximum inductance position. Utilization of the active copper and iron materials within the machine is thus, in principle, relatively poor in the VRM. Second, the VRM essentially operates in a mode in which the field energy is first supplied to and then withdrawn from the machine one phase at a time. No sooner is the field energy supplied to the machine, then it must be rapidly withdrawn from each phase, just as the phase inductance is reaching its maximum to prevent drawing energy from the mechanical system (i.e., producing negative torque). The problem with this limitation lies in the large turn-off inductance, which prevents the current from dropping quickly. This problem of current commutation associated with a large turn-off inductance greatly decreases the torque production capability of the VRM fed by a nonideal power converter with finite kilovoltamperes. This characteristic can be viewed as an additional penalty to the "excitation penalty" normally imposed on all singly excited machines, particularly for small machines. The excitation penalty relates to the fact that the phases of singly excited machines must not only carry the torque producing component of current but must also support the excitation component which serves to magnetize the iron parts. As a result, both the machine windings and the power converter are usually highly stressed from the point of view of voltage and current, resulting in the need for an increased VA rating for the drive. Also, the air gap of the VRM must be substantially reduced compared to competing other machines to help push the machine into the highly saturated region. This requirement adversely offsets the potential low cost advantage of the VRM in addition to causing acoustic noise and torque pulsation. Despite an extensive effort directed at dealing with these practicalities [6], the VRM has thus far fallen short of its theoretical potential in terms of achieving simultaneously good torque density, efficiency, and converter VA ratings. As a result, many researchers view present VRM technology with some skepticism.

Recently, Philips proposed the use of an additional full-pitched winding in the VRM to act as a field winding in an attempt to improve its torque production, based on the concept of premagnetization [7], [8]. The machine of Philips is, in reality, a single stack homopolar inductor machine with the field excitation provided by a full-pitched winding fed from an unipolar converter. This machine configuration has also been explored by the authors from a different perspective [9]. Similar work can be found in an earlier implementation of the concept of premagnetization by Torok in a family of

Paper IPCSD 95–17, approved by the Electric Machines Committee of the IEEE Industry Applications Society for presentation at the 1992 IEEE Industry Applications Society Annual Meeting, Houston, TX, October 4–9. This work received support from the Electrical Power Research Institute (EPRI). Manuscript released for publication February 13, 1995.

Y. Liao was with the Department of Electrical and Computer Engineering, University of Wisconsin, Madison, WI 53706-1691 USA. He is now with General Electric Corporate Research and Development, Schenectady, NY 12301 USA.

F. Liang was with the Department of Electrical and Computer Engineering, University of Wisconsin, Madison, WI 53706-1691 USA. He is now with the Scientific Research Laboratory, Ford Motor Company, Dearborn, MI 48121-2053 USA.

T. A. Lipo is with the Department of Electrical and Computer Engineering, University of Wisconsin, Madison, WI 53706-1691 USA.

IEEE Log Number 9413064.

multiphase reluctance machines he invented [10]. All these machines can be viewed as field-assisted variable reluctance machines, with energy converted primarily through reluctance torque. However, both Philips and Torok failed to recognize the uniqueness brought about by the possible use of PM excitation.

This paper presents a new type of doubly salient motor in which the field excitation is supplied by permanent magnets (PM's) installed in the either the stator or rotor of the motor. This new type of PM motor has evolved from the doubly salient homopolar inductor machine [11] and is therefore termed the *doubly salient permanent magnet (DSPM) motor.* It will be shown that by introducing modern high-performance permanent magnets to advantage in such machines, the above mentioned deficiencies of the VRM are virtually eliminated. The torque production of this motor can then be greatly enhanced. This newly conceived DSPM motor can take on homopolar, rotary magnet, and stationary magnet structures [12], [13]. This paper will focus on the DSPM motor with stationary PM, while the rotary magnet version of the DSPM motor has been described in a previous paper [14].

II. Basic Principles of Operation and Control

A. Configuration of the DSPM Machine

Fig. 1 shows the cross section of a three-phase, 6/4-pole DSPM motor with stationary magnets. This three-phase, 6/4-pole configuration is the most simple pattern for motoring operation requiring satisfactory starting performance. However, two-phase or even single-phase schemes can be conceived for use as a generator. For low speed and high torque applications, the machine can be constructed in repetitive fashion, for example a 12/8 pole configuration.

It can be noted that the rotor of the DSPM machine is identical to that of the three-phase variable reluctance machine. The stator structure is also similar to that of the VRM except that two pieces of PM are buried in the core and therefore introduced into the main flux path of the stator windings. In order to achieve a high flux concentration in such machines, use is made of the corners of the stator lamination which are normally discarded. This changes the physical appearance to either a square or "football" shaped cross section and adds slightly to the weight and space occupied by the machine. High-performance PM material with a linear demagnetizing characteristic is used to sustain the magnetization and demagnetization of the armature reaction so as to keep a nearly constant flux level within the air gap. The stator pole arc is set to be $\pi/6$ mechanical radians, and the rotor pole arc is selected to be slightly greater than the stator pole arc to allow for current reversal. As configured, the air gap reluctance, seen by the PM excitation, is invariant to rotor position if fringing is negligible. Therefore, there is essentially no cogging torque produced at no-load. Ideally, a linear variation of the PM flux linkage and thus a trapezoidal back EMF is induced in each of the stator windings at no-load as shown in Fig. 1.

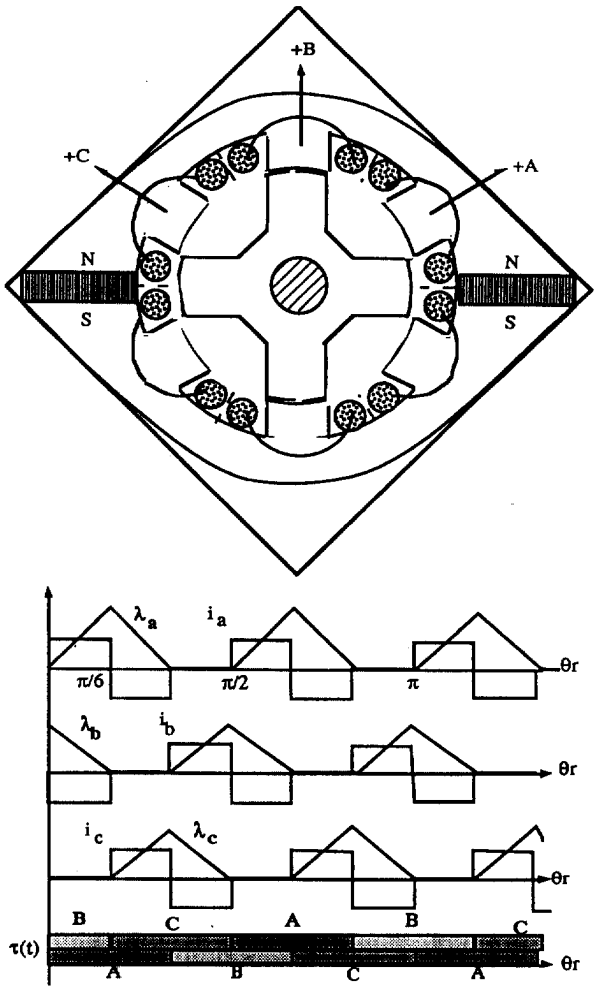

Fig. 1. Illustration of the operating principles of the DSPM motor.

When the machine is loaded, armature reaction flux is produced in the windings in addition to the PM induced flux. It is important to note, however, that the existence of the PM constitutes a very high reluctance path for the armature reaction flux and thus forces the bulk of the armature reaction flux to circulate through another overlapped pole pair. As a result, the active stator phase winding will possess small inductances at *both* the aligned and unaligned positions, and the maximum inductance appears when the poles are, in fact, essentially half overlapped, as illustrated in Fig. 2. In contrast to the VRM, this small aligned inductance makes it possible to reverse the current rapidly at the aligned position. Therefore, torque can be produced both by applying positive current to the winding when its PM-induced flux is increasing and by applying negative current while the flux is decreasing, as shown in Fig. 1.

B. Torque Production in DSPM Machine

The torque expression derived below is based on a simplified linear model for the purpose of illustration. As a first approximation, the variation of the winding inductance and the PM induced flux linkage of an active stator phase winding are assumed to be piece-wise linear and spatially dependent only, as shown in Fig. 2. The terminal voltage equation for an

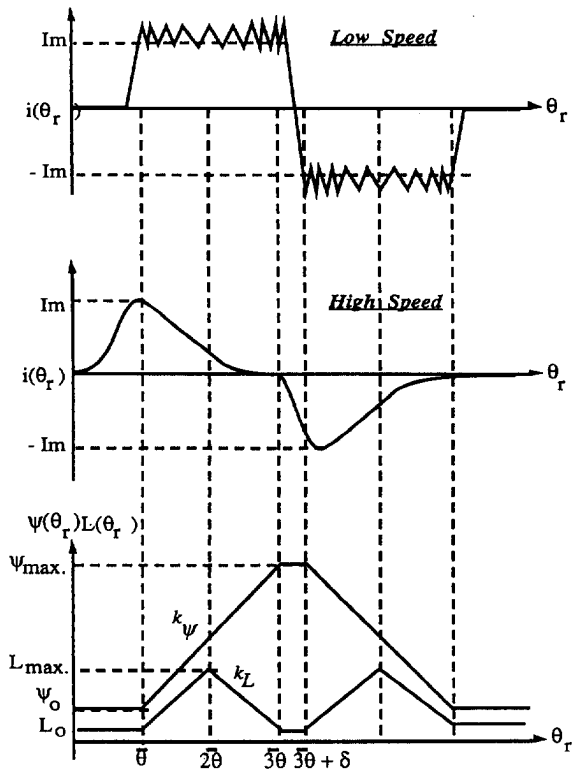

Fig. 2. Current waveforms of the DSPM motor.

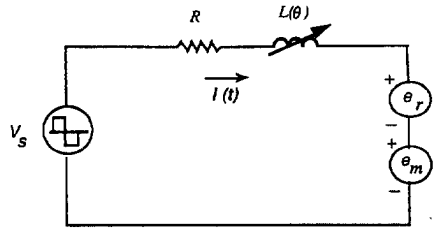

Fig. 3. Equivalent circuit of the DSPM motor.

active stator phase winding is then

$$v = Ri + e \approx e = \frac{d\psi}{dt}. \tag{1}$$

The flux linkage ψ is composed of the PM induced flux linkage ψ_m and the armature reaction flux linkage (Li)

$$\psi = Li + \psi_m. \tag{2}$$

Therefore

$$\begin{aligned} e &= \frac{d\psi}{dt} = L\frac{di}{dt} + i\frac{dL}{dt} + \frac{d\psi_m}{dt} \\ &= L\frac{di}{dt} + e_r + e_m. \end{aligned} \tag{3}$$

This result suggests the equivalent circuit of Fig. 3.

The electrical power entering any of the windings is, neglecting ohmic and iron losses

$$\begin{aligned} \mathcal{P}_e &= ei = iL\frac{di}{dt} + i^2\frac{dL}{dt} + i\frac{d\psi_m}{dt} \\ &= \frac{d}{dt}\left(\frac{1}{2}Li^2\right) + \left\{\frac{1}{2}i^2\frac{\partial L}{\partial\theta_r} + i\frac{\partial\psi_m}{\partial\theta_r}\right\}\omega_r. \end{aligned} \tag{4}$$

Power balance gives

$$\mathcal{P}_e = \frac{d}{dt}\mathcal{W}_f + \mathcal{T}\omega_r. \tag{5}$$

Hence, the torque can be written as the sum of two components

$$\begin{aligned} \mathcal{T} &= \frac{1}{2}i^2\frac{\partial L}{\partial\theta_r} + i\frac{\partial\psi_m}{\partial\theta_r} \\ &= \mathcal{T}_r + \mathcal{T}_m \end{aligned} \tag{6}$$

while the field energy is

$$\mathcal{W}_f = \tfrac{1}{2}Li^2. \tag{7}$$

Careful examination of (6) and (7) reveals the following features of the DSPM motor:

1) The armature reaction field energy $\mathcal{W}_f$, which is to be recovered during current commutation, is very small because of the small value of the stator inductance. Therefore, the energy conversion ratio is very high.
2) Because of the triangular-shaped variation of the stator winding inductance, the reluctance torque $\mathcal{T}_r$ will be small and have a zero average value if the current amplitude is kept constant during one stroke. However, the net reluctance torque will be nonzero if the current varies from the rectangular waveform of Fig. 1.
3) The reaction torque $\mathcal{T}_m$, which is the dominant torque component, can be produced by applying either a positive current to a phase winding when its flux linkage is increasing $(e_m > 0)$ or a negative current when the flux linkage is decreasing $(e_m < 0)$.

It is clear that at low speed, the DSPM motor is, in principle, similar to the PM brushless dc (PM-BLDC) motor with a 120° quasi-square current waveform. The primary difference is that the two 120° conducting current blocks are drawn together in the case of the DSPM motor. It should be realized that a sufficient interval between the two current blocks must be provided in the design of the DSPM motor to ensure current reversal. At high speed, the current cannot be maintained constant due to the excessive PM induced back EMF. In this case, the current peaks in the first half stroke where the inductance is increasing, and drops rapidly in the second half stroke where the inductance is decreasing. This uneven distribution of the phase current, however, is beneficial since it gives rise to a considerable amount of reluctance torque which ultimately contributes to extending the constant power capability of the DSPM motor. This performance advantage clearly distinguishes the DSPM motor from the PM BLDC motor particularly for operation over a wide speed range.

It is interesting to compare the torque production of the DSPM motor with that of the conventional VRM. In this case, both machines are assumed to have identical main dimensions and stator windings. To visualize the difference between the VRM and the DSPM motors, it is helpful to look at the flux versus current loci for both motors, as shown in Fig. 4. Two cases are shown in the graph, one for slightly saturated machines (small machines) and the other for highly saturated machines (large machines). To generate the same copper loss in the two motors, the stator current for the DSPM motor is scaled down to $\sqrt{2}/2$ of that for the VRM. The torque

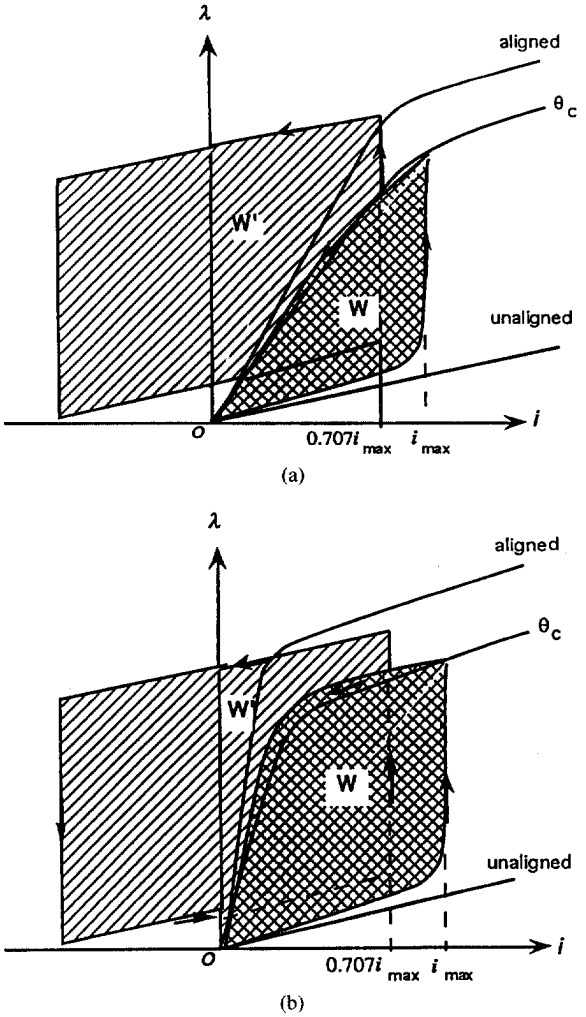

Fig. 4. Comparison of torque production between the VRM and the DSPM motor.

produced in one stroke is represented by the area W for the VRM and W' for the DSPM machine. The area W' is clearly much greater than W due to the fact that: i) The restored field energy, represented by the area R, is only a small fraction of the total field energy; ii) the turn-off angle can be much pushed closer to the aligned position due to the smaller inductance encountered; iii) bidirectional operation brings about a handsome gain in torque production. Assuming the same flux swing, it is very clear that the DSPM motor can achieve ideally between $\sqrt{2}$ to $2\sqrt{2}$ times the torque density of that of the VRM, depending upon how much the SRM suffers from the excitation penalty.

C. Control of the DSPM Motor Drive

The DSPM motor is flexible with regard to converter selection and can be powered either by one of the unipolar converters as typically used for VRM's [6], or by a bipolar converter as used for PM-BLDC motors [15]. Fig. 5 shows a preferred bipolar converter topology with a neutral line to accommodate the additional current which must flow during the commutation period. The DSPM motor drive, as shown schematically in Fig. 5, also features a shaft angle transducer

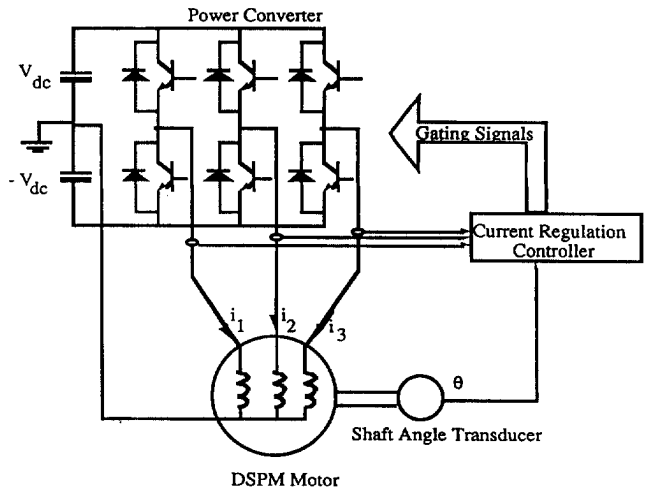

Fig. 5. Schematic diagram of the DSPM motor drive.

to provide rotor position information for control of the stator currents in the normal manner.

Control of the DSPM motor is similar to that of the PM BLDC motor. Four quadrant operation is readily achieved by changing the sequence of conduction and the polarity of the stator currents. Below the base speed, current regulation is preferred to achieve smooth torque production. Above the base speed, the motor becomes voltage fed. Angle control is then utilized in order to realize a constant power range in much the same manner as with a VRM.

III. Nonlinear Analysis of the DSPM Motor

A. Nonlinear Magnetic Analysis

Finite Element Analysis (FEA) is an important tool for accurate steady-state modeling and performance analysis of the DSPM machines, accounting for magnetic saturation, fringing and demagnetization. In [16], the finite element method was applied to the computation of the two-dimensional magnetic field distribution in the cross section of a DSPM machine. The field solution data were then processed to be used for prediction of dynamic and steady-state characteristics of the motor. Experience has shown, however, that the gains by using FEA in the DSPM machine, which has relatively simple geometry, are usually small as compared to the more conventional nonlinear magnetic circuit analysis approach (MCA), particularly for small machines where magnetic saturation is not very severe [16]. It has also been shown that for small frame-size machines, the cross-coupling between the PM flux and the armature reaction flux is quite weak, so that the variations of the PM flux linkage and the armature reaction flux linkage can be assumed to be spatially dependent only.

Nonlinear magnetic circuit analysis has been applied alternatively for this topology to calculate the PM flux linkage and phase inductance variations for purposes of design and dynamic analysis. The no-load PM nonlinear magnetic circuit calculation is quite simple. Calculation of the stator winding inductances is based on the computation of the air gap per-

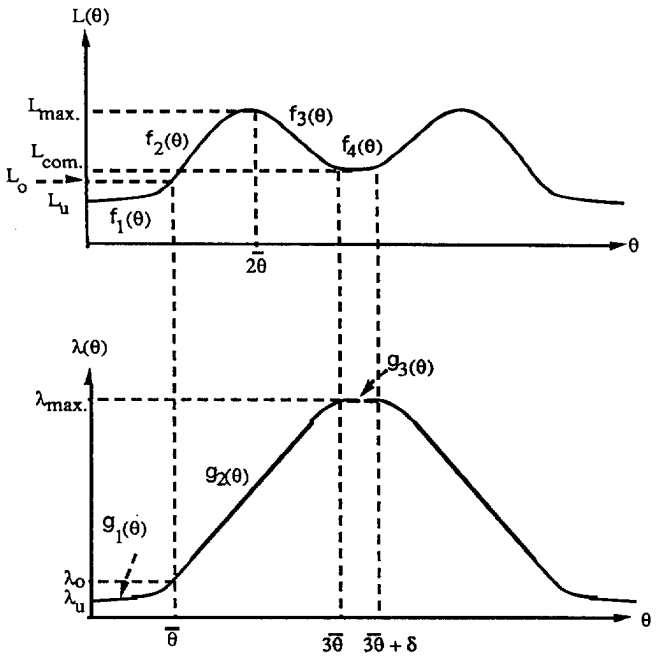

Fig. 6. Variation of (a) the PM induced flux linkage and (b) the winding inductance of the DSPM motor.

meance for a given rotor position, which is well established [16]. The effect of local saturation, when desired, can also be introduced in the calculation of the phase inductance with slight modification, especially for the calculation of the maximum inductance for which the armature reaction is greatest.

As a further simplification, curve-fitting techniques can be used to construct the variations of the PM flux linkage and the armature reaction flux linkage from the calculated values at typical rotor positions, following a similar approach as proposed by Miller for VRM's [17]. Positions of interest include the unaligned, aligned, maximum, and minimum inductance positions, etc. As shown in Fig. 6, the variation of a typical element in the inductance matrix $\mathcal{L}(\theta_r)$ can be approximated by a piece-wise smooth function $\overline{\mathcal{L}}(\theta_r)$

$$f_1(\theta_r) = \mathcal{L}_o + \frac{a(\theta_r - \overline{\theta})}{b - (\theta_r - \overline{\theta})}; \quad 0 \le \theta_r \le \overline{\theta}$$

(Fröhlich-like)

$$f_2(\theta_r) = \mathcal{L}_{\max} - c(\theta_r - 2\overline{\theta})^2; \quad \overline{\theta} \le \theta_r \le 2\overline{\theta}$$

(Parabolic)

$$f_3(\theta_r) = \frac{\mathcal{L}_{\max} - \mathcal{L}_{\text{com}}}{2} \cos\left[\frac{\pi}{\overline{\theta}}(\theta_r - 2\overline{\theta})\right] + \frac{\mathcal{L}_{\max} + \mathcal{L}_{\text{com}}}{2}; \quad 2\overline{\theta} \le \theta_r \le 3\overline{\theta}$$

$$f_4(\theta_r) = \mathcal{L}_{\text{com}}. \quad 3\overline{\theta} \le \theta_r \le 3\overline{\theta} + \delta$$

where a, b, and c can be found from continuity constraints.

The flux linkage variation can then be approximated by $\overline{\lambda}(\theta_r)$ consisting of parabolic and straight lines

$$g_1(\theta_r) = \lambda_o + \frac{a(\theta_r - \overline{\theta})}{b - (\theta_r - \overline{\theta})}; \quad 0 \le \theta_r \le \overline{\theta}$$

(Fröhlich-like)

$$g_2(\theta_r) = \lambda_{\max} - c(\theta_r - 3\overline{\theta}); \quad \overline{\theta} \le \theta_r \le 3\overline{\theta}$$

$$g_3(\theta_r) = \lambda_{\max}. \quad \overline{\theta} \le \theta_r \le 3\overline{\theta} + \delta$$

where a, b, and c can be found from continuity constraints.

B. Dynamic Simulation

The dynamic model of the DSPM motor is derived in the stationary reference frame in phase quantities, with special accounting for the PM. The voltage and flux equations describing the motor are, in matrix form, as follows:

$$\underline{V} = \underline{R}\underline{I} + \frac{d\underline{\Lambda}}{dt} = \underline{R}\underline{I} + \underline{E} \tag{8a}$$

where

$$\underline{V} = \begin{pmatrix} v_1 \\ v_2 \\ v_3 \end{pmatrix}, \quad \underline{I} = \begin{pmatrix} i_1 \\ i_2 \\ i_3 \end{pmatrix}, \quad \underline{E} = \begin{pmatrix} e_1 \\ e_2 \\ e_3 \end{pmatrix}$$

and

$$\underline{\Lambda} = \underline{L}\underline{I} + \underline{\Lambda}_m \tag{8b}$$

with

$$\underline{L} = \begin{pmatrix} \mathcal{L}_{1s} & \mathcal{L}_{12} & \mathcal{L}_{13} \\ \mathcal{L}_{21} & \mathcal{L}_{2s} & \mathcal{L}_{23} \\ \mathcal{L}_{31} & \mathcal{L}_{32} & \mathcal{L}_{3s} \end{pmatrix}, \quad \underline{R} = \begin{pmatrix} \mathcal{R}_1 & 0 & 0 \\ 0 & \mathcal{R}_2 & 0 \\ 0 & 0 & \mathcal{R}_3 \end{pmatrix}, \quad \underline{\Lambda}_m = \begin{pmatrix} \lambda_{m1} \\ \lambda_{m2} \\ \lambda_{m3} \end{pmatrix}.$$

$\underline{L}$ and $\underline{\Lambda}_m$ are assumed to be spatially dependent only, invariant of the stator current. Note that in contrast to the variable reluctance machine mutual inductances appear on the off-diagonal of $\underline{L}$.

From the coenergy method, the equation for the torque can be written as

$$T_e = \frac{\partial \mathcal{W}'}{\partial \theta_r} = \frac{\partial}{\partial \theta_r}\left[\frac{1}{2}\underline{L}\underline{I} + \underline{\Lambda} m^T \underline{I}\right] = \frac{1}{2}\underline{I}^T\left(\frac{\partial}{\partial \theta_r}\underline{L}\right)\underline{I} + \left(\frac{\partial}{\partial \theta_r}\underline{\Lambda} m^T\right)\underline{I}. \tag{9}$$

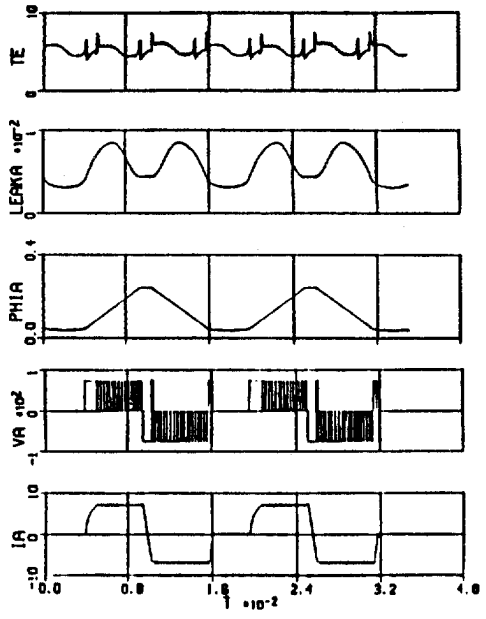

Fig. 7. Simulated waveforms at low speed.

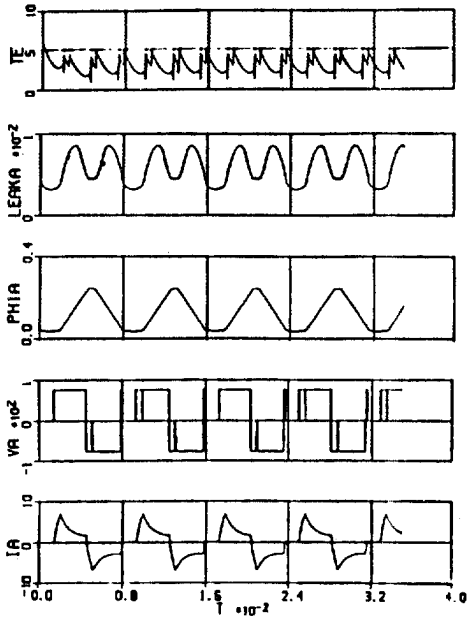

Fig. 8. Simulated waveforms at high speed.

The first term in (9) represents the reluctance torque due to variation of the inductances, and the second term is the reaction torque due to interaction between the winding current and the PM flux.

Equation (8) can be expressed explicitly in terms of either flux linkages or currents to be solved by numerical integration. Note that the elements in the inductance matrix and PM flux linkage vector are all position-dependent quantities as given in Section III-A. The evaluation of torque as per (9) also requires the derivatives of the inductance matrix and PM flux linkages which can be obtained easily from the flux linkage expressions (see Section III-A).

The waveforms of applied voltage and current of a stator phase winding (v_a, i_a) of the prototype DSPM motor and the instantaneous torque produced (T_e) obtained by dynamic simulation for speeds below and above the base speed are shown in Figs. 7 and 8. The variation of the PM induced flux (Phia) and the winding inductance (Leaka) is also shown in the figures. The phase current is kept constant by chopping at low speed. The reluctance torque, as a result, causes a ripple on the top of the torque profile. The build-up and decay of phase currents, especially during the commutating period, contribute to the spikes in the torque waveform. At high speed, the inverter voltage is constant and the active phase winding is turned on at an advanced angle to bring the current to a permissible peak value before the pole pair begins to overlap. The current then begins to collapse, followed by a successful current reversal at the aligned position. The torque ripple content due to reluctance torque is obviously substantial, but the motor can clearly produce a substantial amount of average torque.

IV. Design and Performance of the Prototype DSPM Machine

A prototype DSPM motor has been designed to support the theory outlined above. Design of the DSPM motor is based on a per phase equivalent circuit similar to Fig. 3, with the inclusion of various practicalities [16]. For a meaningful comparison, the prototype machine was designed to have the same outer diameter of stator lamination as that of a 1.0-hp induction motor made by Marathon Electric Co. The frames for both machines are NEMA 145 frames. The stack length is different from the induction machine mainly to accommodate the magnet pieces which were a standard length. The air gap was set to be 0.50 mm. High-energy rare earth permanent magnet material Magnequench II is used. The laminated steel used was 24 Gauge, M19 AISI grade.

The optimal ratio of OD/ID was determined as a result of a design optimization using a nonlinear programming algorithm termed Sequential Quadratic Nonlinear Programming, with the objective function set to be the torque density and the per unit area copper loss the constraint [16]. The tooth flux density and winding current density chosen to be the same as those of the Marathon induction motor, i.e.

$$B_t = 16.5\,\text{kG}$$
$$\text{and } J_s = 3375\ \text{A/in}^2.$$

With this selection, the per unit area stator copper losses in both motors are kept almost the same to place both motors under the same cooling conditions.

A. Inductance Measurements

As a result of experimental tests, the measured maximum air gap flux density of the completed machine was found to be 12.0 kG, which is 20% short of the designed value of 15.1 kG. This reduction is evidently caused by existence of leakage flux paths in the end region and the outer space of the motor, which was not adequately represented in the design program. To compensate for the negative effect on torque production of the machine, the motor was rewound with the stator windings' turns increased by 20%. Number 17-AWG wire was then used instead of 16-AWG. With this change, the

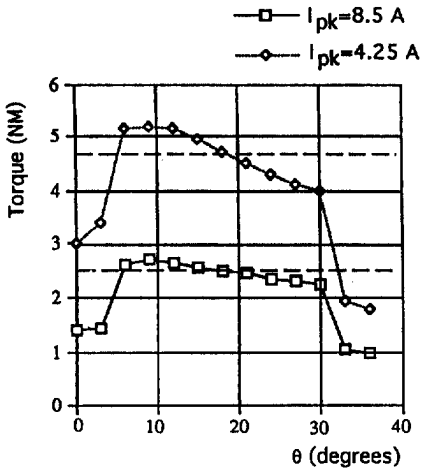

Fig. 9. Static torque profiles of the prototype DSPM motor under 50% and 100% rated current.

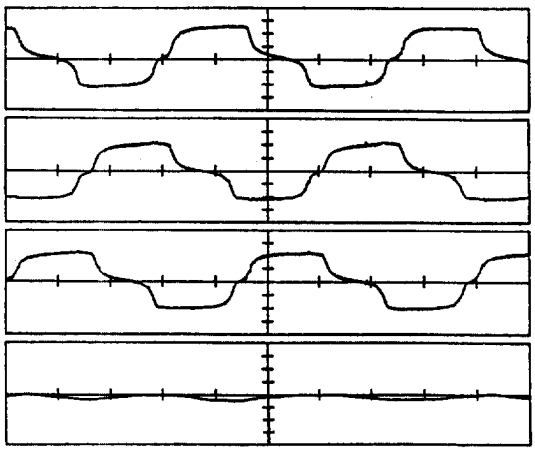

Fig. 10. Oscillogram of the DSPM motor at no load. From the top down: 1) Back EMF of phase A (5 V/div), 2) back EMF of phase A (5 V/div), 3) back EMF of phase A (5 V/div), and 4) shaft torque (1 N · m/div).

stator current density of the prototype DSPM motor is 20% higher than that of the Marathon motor. Consequently, the stator copper loss will be increased by 44%. However, since the Marathon motor has an additional 34% copper loss on the rotor (slip losses), it appears that the per unit area total losses for both machines are now about the same. As a result, the temperature rises of both machines remain about the same.

B. Static Torque Measurement

For static torque measurement, a Sorenson DC Power Supply (DCR 150-12B) is used to supply a dc current to two of the stator phase windings connected in series. A Lebow Strain Gauge torque sensor (Model 1604) together with a Daytronic Signal Conditioner/Indicator (Model 3278) measures the static torque at any locked rotor position. Fig. 9 shows the static torque profiles of the motor over 36° rotor displacement under 50% (4.25 A) and 100% (8.5 A) full-load stator current. The drop of the torque profiles at both ends of the region is due to overlapping of the stator and rotor pole arcs.

From Fig. 9, it can be seen easily that the torque ripple increases almost as current squared. At full load current, the peak of the torque ripple reaches 16% averaged torque. Also it can be seen that at full load current, the averaged torque is 6.0% short of the designed value (5.0 NM), while at 50% current, the machine provides exactly 50% of the designed rated torque. The reason behind this is thought to be the demagnetizing effect of the stator winding currents in the presence of magnetic saturation, similar to the demagnetizing effect of the armature reaction in dc machines.

C. No-load Tests

Under a no-load test, the power converter is switched off and the DSPM motor is driven by the dc motor fed by a Cutler-Hammer Respondor converter. The induced back EMF in each of the stator windings and the shaft torque from the torque transducer can be recorded through a four-channel LeCroy digital oscilloscope. Fig. 10 shows the winding back EMF and the torque waveforms of the experimental DSPM motor at 30% rated speed where the instantaneous torque can be sensed accurately. It can be seen that the back EMF waveforms have a slight slope on top, which is attributable to the imperfect centering of the rotor. The peak value of the back EMF reaches 56.0 V at rated speed (1800 r/min), which meets the design value.

Fig. 12 shows the applied phase voltage, phase current, neutral current and the torque trace of the DSPM motor at 200% rated speed, with the same peak current command of 8.4 A. The difference in the current waveforms at high speed and low speed is very clearly shown, while the neutral current remains relatively small compared to the phase current. It can be seen that the average torque is maintained at about 4.0 N · m up to the rated speed where current regulation is on the verge of disappearing. At speeds higher than the rated speed, the motor enters voltage-fed operation and the averaged torque drops. It is important to mention that the torque transducer cannot reflect the dynamics of torque production of the DSPM motor at high speed due to increased system stiffness at high speed.

D. Efficiency, Torque, and Power Capability

To evaluate the torque and power capabilities and efficiency of the experimental DSPM motor drive, the motor was driven at different speeds with the peak current fixed at 8.5 A. The test was made up to twice rated speed only due to the speed limitations of the test stand. The output power is evaluated by the product of the speed and the measured torque. The input power is obtained by the products of the two dc source voltages and currents. The motor input was read directly from a digital power meter.

The torque and power capability and efficiency curves of the experimental DSPM motor drive are shown in Figs. 13 and 14, with the torque and power normalized to 1 hp. It is very interesting to notice that both output power and efficiency reach a peak at a speed just above rated speed, where chopping terminates and the motor begins picking up reluctance torque. On the other hand, at low speeds where current regulation is maintained by chopping, the output torque

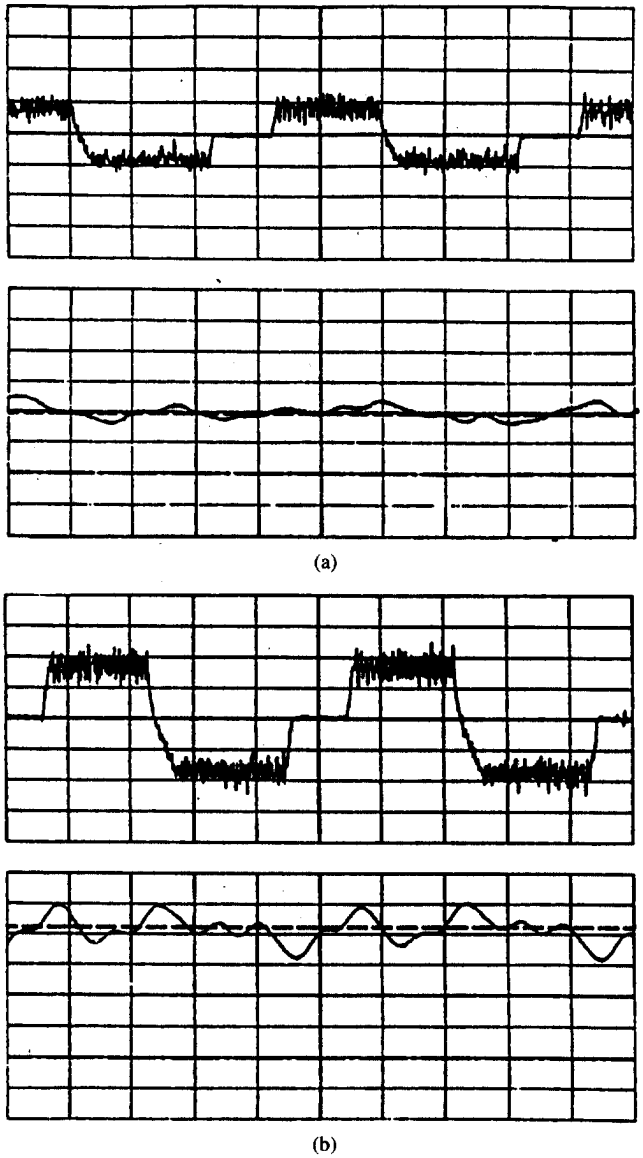

Fig. 11. Current (top trace 5 A/div) and torque (bottom trace 1 N · m/div) waveforms of the DSPM motor at 575 r/min.

is about 20% lower than the design value, while static torque production test suggests only a 6.0% reduction. The additional drop in torque production at rated speed is accompanied by a reduction in efficiency as compared to the design value. Factors causing this discrepancy may be threefold: the larger aligned inductance, the relatively high no-load loss and, more importantly, the existence of stray copper and iron losses due to high-frequency chopping of the winding current which is, of course, an inherent feature of any drive operating from a solid state power converter.

E. Temperature Rise Test

A temperature rise test at rated speed under half load (I_{pk} = 4.25 A) was also carried out on the experimental DSPM motor. The temperatures of the case, magnet, and core were measured using a Barnant 115 Thermocouple Thermometer over a 60-min period. The temperature rise curves for the case

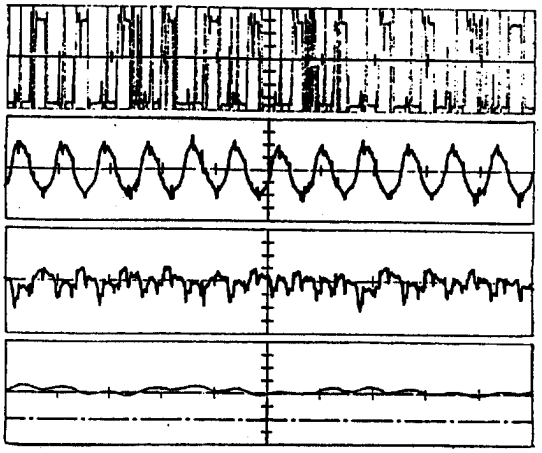

Fig. 12. Oscillogram of the DSPM motor at 3600 r/min. From the top of trace: 1) phase voltage (25 V/div), 2) phase current (5 A/div), 3) neutral current (5 A/div), and 4) shaft torque (1 N · m/div).

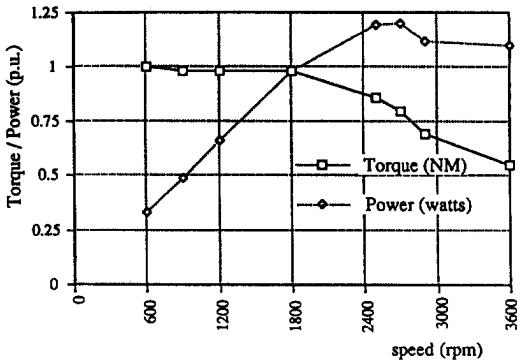

Fig. 13. Capability curves of the DSPM motor.

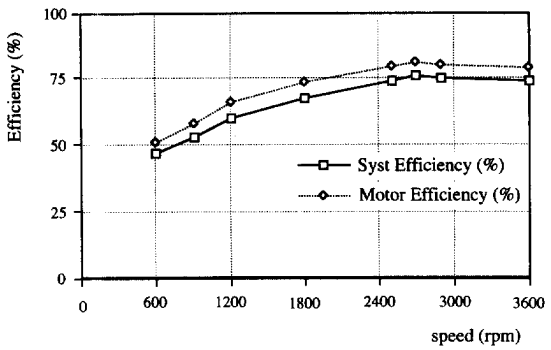

Fig. 14. Efficiency curves for the DSPM motor.

and the core were then projected to full load conditions by multiplying the temperature rises by the ratio of full load total loss to part load total loss, determined from tests to be 1.69. The projected temperature rise curves for full load are shown in Fig. 15. It appears that the temperature rise is quite normal for machines in this range.

Table I summarizes the major performance indices of the prototype motor against the 1-hp Marathon induction motor. Design details of the prototype machine (core depth, tooth depth, etc.) can be found in [16]. It can be seen that with

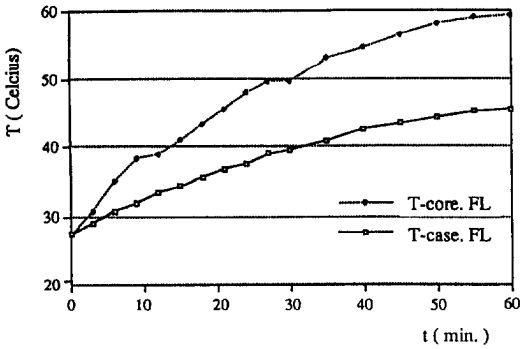

Fig. 15. Projected temperature rise curves for the DSPM motor at full load.

TABLE I
PERFORMANCE COMPARISON BETWEEN INDUCTION MOTOR AND DSPM MOTOR

	DSPM Motor	Induction Motor	DSPM-I (projected)	DSPM-II
Stator OD (mm)	150.	150.	150.	150.
Stack (mm)	30	47.7	47.7	64
Airgap (mm)	0.50	0.30	0.50	0.50
Overall Length (mm) (fan & brgs excl.)	48.	82	66	82
$P_{cu\text{-}sta}$(watts)	72.2	114	90.5	109
P_{loss} (watts)	101.4	232	146	175
Efficiency (%)	90.5	75.0	91.1	91.5
Torque (N-M)	5.0	3.96	7.94	9.44
(%)	126	100	200	248
Torque/Current (%)	134	100	134	134
Torque/Inertia (%)	554	100	554	554

only 3/5 the stack length of the induction machine, the present motor still exceeds the induction machine in torque production, with the efficiency considerably improved. The torque-to-inertia ratio of the DSPM motor is also impressive as can be noted in Table I. To fully appreciate the potential of the DSPM motor, two other projected designs are also included. Design I (DSPM-I), having the same stack length as that of the induction machine, is shown to be able to produce twice the torque as produced by the induction machine, accompanied by a further increased efficiency. Design II (DSPM-II) is set to have the same overall length (length over end winding) as that of the induction machine, with the stack length exceeding that of the induction machine. The DSPM motor can then deliver about 2.5 times the torque and power as that of the induction machine housed in the same frame size.

V. CONCLUSION

This paper has laid the theoretical and experimental foundation for a new type of doubly salient PM machine with stationary permanent magnets. The design and control of these DSPM machines have also been explored but much research work remains ahead to fully assess the potential of such machines. Although the paper treats cylindrical, rotating-field machines, it is evident that the basic principles of the DSPM machine can be employed with advantage to other type of electromechanical devices such as linear machines, axial air gap machines, etc.

The major advantages of the DSPM motor are summarized as follows:

- high torque density and high efficiency,
- simple, rugged structure and high speed capability,
- small VA rating of the power converter as well as the motor,
- low inertia and fast response, and
- low torque ripple and low noise.

The DSPM motor is, however, a pulsed-torque motor by nature, just like the VRM. This feature may prevent the motor from being used for applications where torque quality is critical. Also, special consideration should be given to reduce the demagnetization effect of armature reaction in large machines.

In general, with its superior performance in torque production and structural simplicity, the DSPM motor drive could serve as a potential alternative to existing servo and industrial ac motor topologies, especially in small frame sizes, for variable speed drives. It is especially suitable for applications where size and weight are critical.

ACKNOWLEDGMENT

The authors thank Y. Zhao of the University of Wisconsin, Madison, for help during the construction and testing of the power converter and drive, W. Dittman of Marathon Electric Co. for providing the details of the induction motor and assisting in building the prototype DSPM machine, and Dr. N. Boules of GM-Research Laboratory for providing the permanent magnet material Magnequench II.

REFERENCES

[1] P. J. Lawrenson, J. M. Stephenson, P. T. Blenkinsop, J. Corda, and N. N. Fulton, "Variable speed switched reluctance motors," *Proc. IEE,* vol. 127, pt. B, pp. 253–65, July 1980.
[2] W. F. Ray, P. J. Lawrenson, R. M. Davis, J. M. Stephenson, N. N. Fulton, and R. J. Blake, "High performance switched reluctance brushless drives," *IEEE Trans. Ind. Applicat.*, vol. IA-22, no. 4, pp. 722–30, 1986.
[3] J. M. Stephenson and R. J. Blake, "The design and performance of a range of general-purpose industrial SR drives for 1 KW to 110 KW," in *IEEE Ind. Applicat. Soc. Annu. Meeting,* 1989, pp. 99–107.
[4] S. R. McMinn, "Control of the switched reluctance machine," in *Switched Reluctance Drives, IEEE Ind. Applicat. Soc. Tutorial,* 1990.
[5] E. Richter, "Switched reluctance machines for high performance operation in a harsh environment—A review paper," presented at the Int. Conf. Electrical Machines, Cambridge, MA, Aug. 12–15, 1990.
[6] A. Hava, V. Blasko, and T. A. Lipo, "A modified C-dump circuit for variable reluctance machines," in *IEEE Ind. Applicat. Soc. Annu. Meeting,* 1991, pp. 886–91.
[7] D. A. Philips, "Switched reluctance drives: New aspects," in *IEEE Power Electron. Specialist Conf. (PESC),* 1989, pp. 579–584.
[8] ——, "A novel high performance-low noise switched reluctance motor," in *Int. Conf. Electrical Machines,* Cambridge, MA, Aug. 12–15, 1990.
[9] F. Liang, Y. Liao, and T. A. Lipo, "Variable reluctance motor with auxiliary commutating winding," submitted for publication at *IEEE Ind. Applicat. Soc. Annu. Meeting,* Houston, TX, Oct. 1992.
[10] V. Torok, "Electrical reluctance machine," U.S. Patent 4 349 605, 1982.
[11] J. H. Walker, "The theory of the inductor alternator," *J. IEE,* vol. 89, pt. II, pp. 227–241, 1942.
[12] T. A. Lipo and Y. Liao, "A new class of variable reluctance motors with permanent magnet excitation," U.S. Patent pending.

[13] T. A. Lipo, Y. Liao, and F. Liang, "A new doubly salient permanent magnet motor with stationary magnet," U.S. Patent pending.
[14] Y. Liao and T. A. Lipo, "A new doubly salient permanent magnet motor for adjustable speed drives," presented at SPEEDAM, Italy, May 1992.
[15] T. J. E. Miller, *Brushless PM and SR Drives.* Oxford, England: Clarendon, 1989.
[16] Y. Liao, "Design and performance evaluation of a new class of permanent magnet machines with doubly salient structure," Ph.D. thesis, University of Wisconsin, Madison, Dec. 1992.
[17] T. J. E. Miller *et al.*, "Design of a synchronous motor drive," *IEEE Trans. Ind. Applicat.*, vol. 27, no. 4, pp. 741–749, July/Aug. 1991.

Yuefeng Liao (S'91–M'92) is a native of Canton, P.R.C. He received the B.S. and M.S. degrees in electrical engineering in 1983 and 1986, respectively, from Tsinghua University, Beijing, P.R.C., and the Ph.D. degree in electrical engineering from the University of Wisconsin, Madison, in 1992.

He was a lecturer at the South China University of Technology, Canton, from 1986 to 1988, and an Engineering Specialist with Emerson Motor Technology Center, Emerson Electric Company, St. Louis, MO, from 1992 to 1994. He is presently a Staff Electrical Engineer at the Corporate Research and Development Center, General Electric Company. His interests are mainly focused on new ac motor and drive system development and their applications. He has published some 20 papers in this area. He is the recipient or corecipient of several U.S. patents.

Dr. Liao received a Second-Prize Paper Award from the IEEE Industry Applications Society in 1994, a First-Prize Paper Award from the Industrial Drives Committee at the 1993 IEEE Industry Applications Society Annual Meeting, and a Second-Prize Paper Award from the Electric Machines Committee at the 1992 IEEE Industry Applications Society Annual Meeting. He serves on the Industrial Drives Committee and the Electric Machines Committee of the IEEE Industry Applications Society.

Feng Liang (S'91–M'93) was born in Nanning, P.R.C. He received the B.S. and M.S. degrees in 1982 and 1986, respectively, from the South China University of Technology, P.R.C., and the Ph.D. degree from the University of Wisconsin, Madison, in 1993, all in electrical engineering.

He then joined the Scientific Research Laboratory, Ford Motor Company, as an Engineering Specialist. His current research interests include the design, modeling, simulation, and control of electromagnetic devices and electric drives.

Dr. Liang has received three IEEE prize paper awards, including being corecipient of the Best Paper Award in the IEEE TRANSACTIONS ON INDUSTRY APPLICATIONS for 1993.

Thomas A. Lipo (M'64–SM'71–F'87) is a native of Milwaukee, WI. He received the B.E.E. and M.S.E.E. degrees from Marquette University, Milwaukee, in 1962 and 1964, respectively, and the Ph.D. degree in electrical engineering from the University of Wisconsin, Madison, in 1968.

From 1969 to 1979, he was an Electrical Engineer in the Power Electronics Laboratory, General Electric Corporate Research and Development, Schenectady, NY. He became Professor of Electrical Engineering at Purdue University, West Lafayette, IN, in 1979. In 1981, he joined the University of Wisconsin, Madison, in the same capacity, and where he is currently the W. W. Grainger Professor for Power Electronics and Electrical Machines. He has been engaged in power electronics research for over 30 years.

Dr. Lipo has received 18 IEEE prize paper awards for his work, including being corecipient of the Best Paper Award in the IEEE TRANSACTIONS ON INDUSTRY APPLICATIONS for 1984 and 1994. In 1986, he received the Outstanding Achievement Award for his contributions to the field of ac drives, and in 1990, received the William E. Newell Award from the IEEE Power Electronics Society for contributions to the field of power electonics. In 1994, he received the Nicola Tesla Award from the Power Engineering Society for his work in electrical machinery. He served as President of the IEEE Industry Applications Society in 1994.